Eur. Phys. J. B **47**, 443–447 (2005)
DOI: 10.1140/epjb/e2005-00345-6

The European Physical Journal B

Multiple-frequency current oscillations in GaAs-AlGaAs quantum wells containing a thin semi-insulating layer

Z.H. Dai[1,2,a] and J. Ni[1]

[1] Department of Physics and Key Laboratory of Atomic and Molecular Nanoscience, Tsinghua University, 100084, Beijing, P.R. China
[2] Department of Physics, Yantai University, 264005, Yantai P.R. China

Received 14 March 2005 / Received in final form 23 May 2005
Published online 28 October 2005 – © EDP Sciences, Società Italiana di Fisica, Springer-Verlag 2005

Abstract. We have investigated non-equilibrium electron transport properties of a quantum well with an inserted thin semi-insulating potential barrier layer in nonlinear bias using a time-dependent simulation technique. We find that the charge redistribution with time in the whole structure has an important effect on the final current-voltage (I-V) curves. The results show that there are two evident current hysteresis phenomena in the negative differential conductance regions and the inserted semi-insulating potential barrier layer induces the formation of multiple emitter quantum wells, which leads to high-frequency terahertz current oscillations with multiple-frequency relations around the valley of current.

PACS. 73.63.Hs Quantum wells – 73.21.Fg Quantum wells – 73.23.-b Electronic transport in mesoscopic systems – 73.50.-h Electronic transport phenomena in thin films

Double-barrier resonant tunneling nanostructures have been extensively studied due to their potential device applications. There have been many important experimental discoveries in this confined system [1–5]. Most of the experimental research focuses on the dc transport properties, such as linear and nonlinear response [6–8]. Because of the small dimension of the nanostructure device, a very small bias voltage applied on the device can cause a very strong internal electric field. Thus, the carriers in the device are in a state far from the equilibrium state. Besides this, the transport processes become non-Markovian due to memory effects induced by scattering, some abnormal phenomena have been found, such as the negative current problem under positive bias [9]. The effects of transient current transport and charge density variations in the non-equilibrium states are still a important problem.

In this paper, using a time-dependent simulation technique, we study the electron transport behaviour of a main AlGaAs/GaAs/AlGaAs quantum well with a thin semi-insulating potential barrier layer which can be formed by adequate doping with Al atoms in the GaAs quantum well. The band-profile is shown in the inset of Figure 1. Similar structures have been fabricated in experiment, such as resonant tunneling diodes that incorporate a single layer of InAs quantum dots [10,11], as well as a monolayer InAs potential well or AlAs potential barrier [12,13]. The experimental current-voltage (I-V) curve of electron transport through a double-barrier AlGaAs/GaAs/AlGaAs quantum-well shows bistability and a plateaulike structure [14–16]. In our theory, we obtain the high-frequency oscillations of current as well as a multiple-frequency oscillation relation, which occur in the first and second I-V hysteresis cycles, respectively. The high-frequency oscillations of current in double-barrier structures have been introduced in some experimental and theoretical studies [16–18], and current oscillations with frequencies below THz have also been detected in experiment [16]. Our work obtains the multiple-frequency relation of current oscillation in the double barrier structure with a thin semi-insulating layer whose steady state I-V curves have been obtained in experiment [14]. This kind of current hysteresis has also been found in the quantum wells of many other materials [19–23].

The inserted layer can introduce charge redistribution to form multiple emitter quantum wells and has an important effect on the current transport in the device. We find two high-frequency current oscillation regions in which there are current multiple-frequency oscillations. These time-dependent nonlinear characteristics may find application in future high-frequency devices.

The Wigner function formulation of quantum mechanics has been used in our approach due to its ability to handle dissipated and open-boundary systems naturally [17,18,24]. This equation is not the steady state but a time-dependent equation, which considers the time effect. The detailed theoretical method can be found in reference [25]. With the lowest-order approximation to the

[a] e-mail: zhdai@ytu.edu.cn

scattering term, the time-dependent dynamic equation for quantum transport is

$$\frac{\partial f(x,k)}{\partial t} = -\frac{\hbar k}{m^*}\frac{\partial f(x,k)}{\partial x} - \frac{1}{\hbar}\int_{-\infty}^{\infty}\frac{dk'}{2\pi} f(x,k') V(x,k-k') + \left.\frac{\partial f(x,k)}{\partial t}\right|_{coll}, \quad (1)$$

where the kernel of the potential operator is given by

$$V(x,k-k') = \int_0^L dr \sin[(k-k')r] \times [U(x+r/2) - U(x-r/2)]. \quad (2)$$

m^* is the electron effective mass. x and r are the Wigner-Weyl transformation coordinates. U is the conduction-band edge. $f(x,k)$ is the Wigner function. Appropriately treating scattering in semiconductors is very important for getting reasonable simulation results. We employ the relaxation-time approximation to deal with the scattering. In the relaxation time approximation, the collision terms in the above equation are written as

$$\frac{\partial f(x,k)}{\partial t} = \frac{1}{\tau}\left[\frac{f_0(x,k)}{\int f_0(x,k)\ dk}\int f(x,k)\,dk - f(x,k)\right], \quad (3)$$

where τ is the relaxation time and f_0 is the equilibrium Wigner function. The boundary conditions are

$$f_{x=0,k>0} = \frac{m^* k_B T}{\pi\hbar^2} \times \ln\left\{1 + \exp\left[-\frac{1}{k_B T}\left(\frac{\hbar^2 k^2}{2m^*} - \mu_0\right)\right]\right\}, \quad (4)$$

$$f_{x=L,k<0} = \frac{m^* k_B T}{\pi\hbar^2} \times \ln\left\{1 + \exp\left[-\frac{1}{k_B T}\left(\frac{\hbar^2 k^2}{2m^*} - \mu_L\right)\right]\right\}. \quad (5)$$

The corresponding electron and current density may be obtained by the k-space integral of the Wigner function. Another important equation in our model is the Poisson Equation (PE). Because of the conservation of the transverse momentum, the electron density in the plane vertical to the electron transport direction is distributed homogeneously. So the Poisson equation in our model is reduced into a one-dimensional equation where the x direction is the electron transport direction,

$$\frac{d^2}{dx^2}u(x) = \frac{q^2}{\varepsilon}\left[N_d(x) - n(x)\right], \quad (6)$$

where ε is the dielectric permittivity. $u(x)$ is the electrostatic potential, q is the electronic charge, $N_d(x)$ is the concentration of ionized dopants, and $n(x)$ is the density of electrons, which is given by

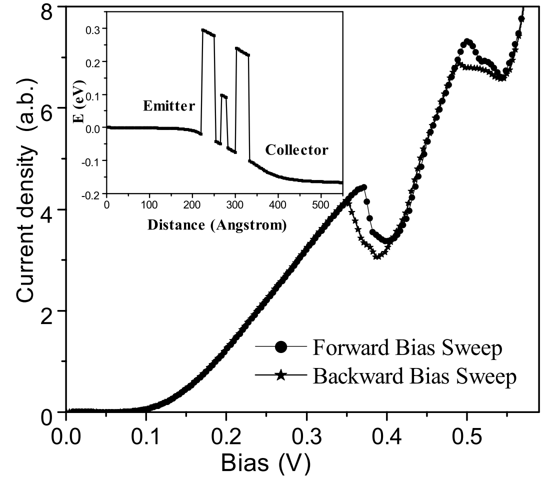

Fig. 1. I-V curves of the double-barrier structures with an inserted potential barrier layer, the data are the time-averaged values of current. The inset is the conduction-band diagram of device under certain bias.

$$n(x) = \int_{-\infty}^{\infty}\frac{dk}{2\pi} f(x,k). \quad (7)$$

The corresponding current density may be written as

$$j(x) = \int_{-\infty}^{\infty}\frac{dk}{2\pi}\frac{\hbar k}{m^*} f(x,k). \quad (8)$$

To solve the WFE-PE equations, we must discretize the simulation zone and these WFE-PE equations. The final results of the current and electron density are obtained by self-consistent calculations [25].

The parameters used in our simulations are as follows: The momentum and position spaces are discreted into 134 and 160 points, respectively. The donor density is $N_d = 2.0 \times 10^{18}$ particles/cm^3, and the doping extends to 3.0 nm before the emitter barrier and after the collector barrier. The compensation ratio for scattering calculations is 0.3. The high emitter and collector $Al_xGa_{1-x}As$ potential barrier, undoped GaAs main quantum well and thin inserted semi-insulating Al_yGa_{1-y} As potential barrier widths are 3.0, 5.0 and 1.38 nm, respectively, as shown in the inset of Figure 1. The simulation box is 55.0 nm and the main barrier potential is 317 meV. The device temperature is 77 K. The effective mass of an electron is taken to be 0.0667 m_0.

Figure 1 shows the mean I-V curves of the quantum well with the inserted potential barrier layer when the time-dependent simulation reaches steady state in the forward and backward bias sweeps. In the calculation, the bias voltage is applied to the device continuously with a 2 ps time interval for each bias step. There is a transient regime for each bias step, but the final current value is a mean value of transient current. According to our calculation, the transient irregular current occurs in the first 200 fs interval, the current can basically reach the

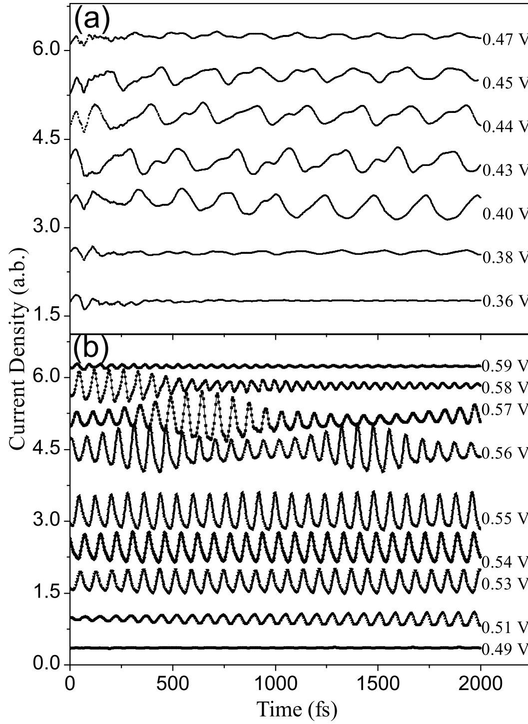

Fig. 2. The current density as a function of time in the forward bias sweep. (a) under low bias which corresponds to the first resonance bias, (b) under high bias which corresponds to the second resonance bias. For clarity of presentation, all the curves have been translated in the vertical coordinate by certain values.

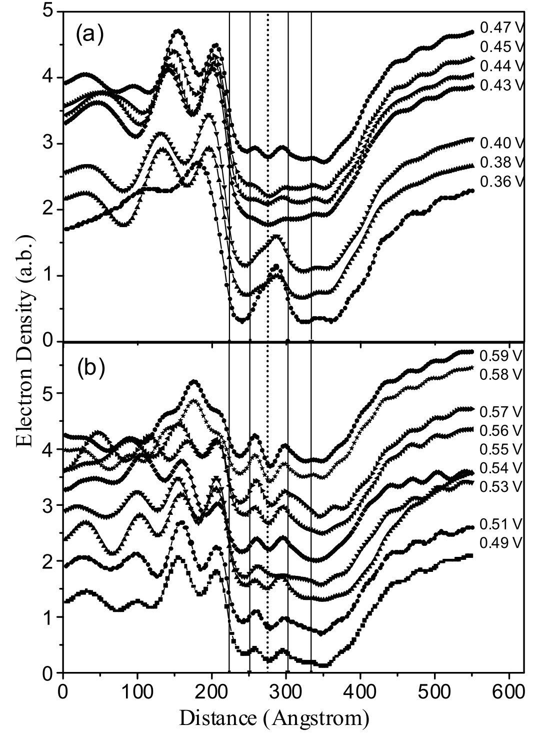

Fig. 3. The local electron density distributions in the forward bias sweep. (a) under low bias which corresponds to the first resonance bias, (b) under high bias which corresponds to the second resonance bias. For clarity of presentation, all the curves have been translated in the vertical coordinate by certain values.

steady state, which shows either a sustaining oscillation or a constant value. The I-V curve shows two evident current hysteresis regions, as is shown in Figure 1. When we consider the time-dependent current density, the results show the following phenomena: (1) the current density shows an oscillation with the frequency of about 4 THz; (2) the multiple-frequency oscillations of current density appear in different bias voltage regions; (3) The current density oscillations with time show amplitude-modulated wave form; (4) the current density oscillations mainly lie around the valleys in the hysteresis regions.

The time-dependent current density curves at different bias voltages of the forward bias sweep are shown in Figure 2. The current density oscillation with the frequency of about 4 THz appears after the bias voltage passes the resonant bias voltage (0.38 V). With increasing bias voltage, the peaks of current density start to split and the double-frequency phenomenon appears. When the current is far from the valley, it returns to a linear response. The second hysteresis region appears when the bias voltage equals 0.5 V. We find that a triple-frequency current oscillation of about 12 THz appears in this region, as shown in Figure 2b. In order to understand these phenomena, we have analysed the distribution of the electron density as shown in Figure 3. From Figure 3a, it can be seen that in low bias voltage which corresponds to the first resonant tunneling of the devices, there is an electron density peak in the main quantum well (MQW) and there are no evident electron density oscillations in the emitter region before the emitter potential barrier. In this bias voltage region, the emitter quantum well (EQW) is not formed. However, when the bias voltage passes the resonant point, the sudden decrease in the tunnelling current leads to a dramatic increase in the electron reflection coefficient. The interference between the injected and reflected electron waves causes a large spatial depletion of electron density in the emitter region. The depletion of electrons induces a drop in the potential and forms an EQW. Also the depth of the EQW increases with the increase of the bias voltage, and the energy level of the EQW separates from the three-dimensional continuum states in the emitter region. The coupling between the conduction-band edge in the EQW and the lowest-energy level in the MQW tends to lift the energy level in the MQW and depresses the conduction-band edge in the EQW. The applied bias has the opposite effect on the energy level in the MQW. The interplay of these two opposite effects determines the formation of the EQW. The existence of the inserted thin barrier layer adjusts the energy level structure of the MQW by restricting the electron motion of the MQW, which further affects the electron density distribution of the emitter region and forms the multiple EQWs as shown in Figure 3. Furthermore, the coupling between the energy level in the EQWs and that in the MQW will

greatly influence the transport of electrons. There are several factors jointly affecting the transport process: the coupling between the three-dimensional continuum states and the level of MQW contributes the main current, and the coupling between the level of EQW and that of MQW provides the accessional current forming the oscillatory current density. Coupling between multi-EQWs and MQW will leads to the multi-frequency current density oscillations. This coupling of the EQW and MQW contributes to the current oscillations, so the formation of an emitter quantum well is important. Because of the large capacitance and impedance of the device, it might be difficult to detect directly the high-frequency oscillations of current using the electric detection technique. But, the EQW is formed mainly through the time-dependent change of electron density in the emitter close to the $\mathrm{Al}_x\mathrm{Ga}_{1-x}\mathrm{As}$ barrier. This change of electron density in emitter can affect the photoluminescence or absorption spectrum and make it change with time. The high-velocity femtosecond laser technique can be used to detect this kind of charge density change in the emitter, so that information concerning the electron density in the emitter through photoluminescence or absorption spectrum change can be obtained.

In order to explain these kind of current density oscillations, we give the following qualitative explanation using a less rigorous, yet transparent theoretical model. Because the energy level in the EQW is a quasi-bounded state, we suppose that the average residence times of electrons in the EQW and MQW are $\hbar/\gamma_E$ and $\hbar/\gamma_M$, respectively, where γ_E and γ_M are the corresponding quasi-bound energies of the EQW and MQW. After the formation of the EQW, the electrons can inject into the EQW and occupy the quasi-bound state level by phonon scattering. When the level of the EQW is close to that of the MQW, the electrons of EQW can tunnel into the MQW which leads to accessional electron transport. However, at this time, the velocity of injected electrons is larger than that of tunneling electrons, and electron injection is dominant, which leads to electron accumulation and lifts the conduction-band edge and quasi-bound state level. The lifted level of the EQW promotes the electron transport, and the current increases gradually. When the level of the EQW equals that of the MQW, electron tunnelling is dominant. The tunneling of electrons into the MQW makes the electron number in the EQW decrease and reduces the conduction-band edge of the EQW, which leads to a decrease of tunneling current until the injected electrons are re-dominant, and a new accessional current cycle starts. So the current oscillation is determined by the average residence time of electrons in the quasi-bound state level. When only one EQW is formed, the coupling between the EQW and the MQW makes the residence time of electrons in the coupling system be $\hbar/(\gamma_E + \gamma_M)$. Because $\gamma_M << \gamma_E$, the oscillation period is the electron average residence time $\hbar/\gamma_E$ in the EQW, and the residence time of electrons in the MQW can modulates this oscillation frequency as shown in Figure 2b. When there are two EQWs, the residence time is $\hbar/(\gamma_{E1} + \gamma_{E2})$. Because the level coupling between the EQWs is large only when the two levels of EQWs are near, i.e. $\gamma_{E1} = \gamma_{E2}$, the oscillation frequencies are doubled. Thus, the multiple-frequency oscillations of current are related to the number of EQWs and requires that the levels of the different EQWs are near. When the bias further increases to reach the second hysteresis region, the emitter region shows a three-EQW structure, which leads to triple-frequency current oscillations. According to our explanations, the current oscillation frequency is determined by the parameters of the device, such as the width and height of barrier and width of quantum well and middle semi-insulating barrier layer, but the relation of multiple-frequency does not depend on the detailed device parameters. At the same time, the coexistence of the 3D and 2D states in the emitter is necessary for the formation of the oscillations, so the spacer region and doping concentration is also very important. Its oscillation amplitude could depend on the height and width of middle barrier, but it needs further studies.

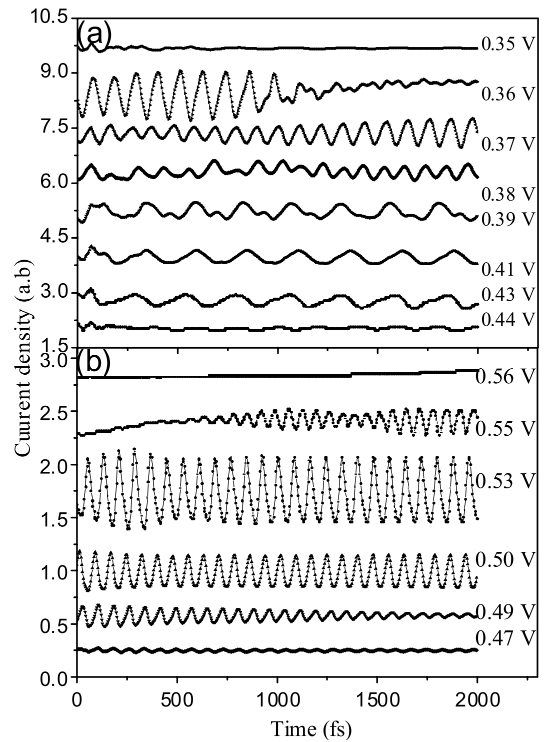

Fig. 4. The current density as a function of time in the backward bias sweep. (a) under low bias which corresponds to the first resonance bias, (b) under high bias which corresponds to the second resonance bias. For clarity of presentation, all the curves have been translated in the vertical coordinate by certain values.

Figure 4 represents the current as a function of time in the backward bias sweep, which shows a similar phenomenon. The forward bias sweep corresponds to the injection process. The backward bias sweep corresponds to the electron drag process, which is not the simple inverse process in the situation of non-equilibrium electron transport. In backward sweep, the double-frequency phenomenon is more significant and appears in the low bias as shown in Figure 4a.

In conclusion, for the quantum well device with an inserted thin potential barrier layer, we have found two evident current hysteresis regions and multiple-frequency oscillations of current density. This inserted potential barrier layer strongly affects the electron density distribution and current curves. It promotes the formation of multi-EQWs in the emitter region and further leads to current density oscillations. Using this inserted layer technique, we can adjust the high-frequency oscillations only by changing the dc bias voltage, which leads to a multiple-frequency quantum device only by changing the bias between the device. In the future, experimental researchers may use high-velocity femtosecond lasers to detect the change of electron density in the emitter close to the barrier to obtain information about these high-frequency oscillations. These results can extend qualitatively to the case of a quantum well with a repulsive potential quantum-dot layer.

We thank Prof. H.L. Cui and Dr. Peiji Zhao of Steven Institute of Technology, USA, for help in the calculation method. The work was supported by the National Basic Research Program of China (Grant No. G2000067107) and the National Foundation of Natural Science in China (Grants No. 10404022).

References

1. A.D. Martin, M.L.F. Lerch, P.E. Simmonds, L. Eaves, Appl. Phys. Lett. **64**, 1248 (1994)
2. R.K. Kawakami, E. Rotenberg, H.J. Choi, E.J. Escorcia-Aparicio, M.O. Bowen, J.H. Wholfe, E. Arenholz, Z.D. Zhang, N.V. Smith, Z.Q. Qiu, Nature **398**, 132 (1999)
3. D. Grundler, Phys. Rev. Lett. **84**, 6074 (2000)
4. H.C. Liu, C.Y. Song, Z.R. Wasilewski et al., Phys. Rev. Lett. **90**, 077402-1 (2003)
5. D. Snoke, S. Denev, Y. Liu, L. Pfeiffer, K. West, Nature **418**, 754 (2002)
6. R. Gebauer, R. Car, Phys. Rev. B **70**, 125324-1 (2004)
7. N. Tansu, J.Y. Yeh, L.J. Mawst, Appl. Phys. Lett. **83**, 2112 (2003)
8. T. Ohtsuka, L. Schrottke, R. Hey, H. Kostial, H.T. Grahn, J. Appl. Phys **94**, 2192 (2003)
9. H. Ikeda, M. Iwasaki, Y. Ishikawa, M. Tabe, Appl. Phys. Lett. **83**, 1456 (2003)
10. A. Rosenauer, D. Gerthsen, D. Van Dyck, M. Arzberger, G. Böhm, G. Abstreiter, Phys. Rev. B **64**, 245334 (2001)
11. F. Pulizzi, E.E. Vdovin, K. Takehana, Yu.V. Dubrovskii, A. Patane, L. Eaves, M. Henini, P.N. Brunkov, G. Hill, Phys. Rev. B **68**, 155315 (2003)
12. G.B. Galiev, V.E. Kaminskii, V.G. Mokerov, V.A. Kulbachinskii, R.A. Lunin, I.S. Vasilevskii, A.V. Derkach, Semiconductors **37**, 686 (2003)
13. Z. Barticevic, P. Vargas, M. Pacheco, D. Altbir, Phys. Rev. B **68**, 155306 (2003)
14. P.M. Martin, S.A. Ahmad, F.W. Sheardt et al., Semicond. Sci. Technol. **9**, 493 (1994)
15. V.J. Goldman, D.C. Tsui, J.E. Cunningham, Phys. Rev. Lett. **58**, 1256 (1987)
16. T.C.L.G. Sollner, Phys. Rev. Lett. **59**, 1622 (1987)
17. K.L. Jensen, F.A. Buot, Phys. Rev. Lett. **66**, 1079 (1991)
18. Peiji Zhao, H.L. Cui, D.L. Woolard, Phys. Rev. B **63**, 075302 (2001)
19. P.C. Main, T.J. Foster, P. Medonnell, L. Eaves, M.J. Gompertz, N. Mori, J.W. Sakai, M. Henini, Phys. Rev. B **62**, 16721 (2000)
20. M. Roberts, Y.C. Chung, S. Lyapin, N.J. Mason, R.J. Nicholas, P.C. Klipstein, Phys. Rev. B **65**, 235326 (2002)
21. L. Hirsch, A.S. Barriere, J. Appl. Phys **94**, 5014 (2003)
22. G. Kim, D.W. Roh, S.W. Paek, Appl. Phys. Lett. **83**, 695 (2003)
23. A. Yu. Serov, G.G. Zegrya, Appl. Phys. Lett. **86**, 032108 (2005)
24. R.P. Zaccaria, F. Rossi, Phys. Rev. B **67**, 113311 (2003)
25. Z. Dai, J. Ni, Eur. Phys. J. B **45** 129 (2005)